J Intell Robot Syst (2016) 81:505–529
DOI 10.1007/s10846-015-0236-9

Cooperative Tracking a Moving Target Using Multiple Fixed-wing UAVs

Mingfeng Zhang · Hugh H. T. Liu

Received: 3 April 2014 / Accepted: 27 April 2015 / Published online: 13 June 2015

Abstract A cooperative tracking scheme is presented in this paper for multiple fixed-wing unmanned aerial vehicles (UAVs) to track an uncooperative, moving target. It is comprised of a target loitering algorithm and a formation flight algorithm. The loitering algorithm enables a constant speed UAV to circle around a moving target, whose speed is allowed to vary up to the UAV's speed. The formation algorithm enables cooperative tracking using multiple UAVs by keeping them flying in a circular formation with equal inter-vehicle angular separation. Under this formation algorithm, the formation center can be controlled independently to perform target loitering, and the admissible range of the target's speed would not be affected for given UAVs. The performance of the proposed tracking system is verified in numerical simulations.

Keywords Target tracking · UAV · Formation

1 Introduction

Tracking a moving target is a key function of unmanned aerial vehicles (UAVs) [1]. It is required in a wide range of UAV applications, such as reconnaissance, surveillance, and target acquisition. It is also a very challenging task if manually operated; therefore, automating this process has significant implications. It could greatly improve the overall autonomy of UAVs, thus reliving the burden of UAV operators and improving the efficiency and safety of UAV missions. The goal of this paper is to develop a target tracking system that allows multiple fixed-wing UAVs to cooperatively track a ground moving target (GMT).

A great challenge involved in the UAV-GMT tracking problem stems from the maneuverability disparity between these two different types of vehicles. Contrary to the great maneuverability that GMTs usually exhibit, the motion of fixed-wing UAVs is subject to various kinematic constraints. GMTs can be very agile and vary their speeds quickly over a large range, while fixed-wing UAVs cannot hover and must maintain forward motion to stay in the air. Besides, the turning radius of fixed-wing UAVs is much larger than that of GMTs. In order to overcome this challenge, previous work usually approached UAV-GMT tracking problems by introducing a predefined tracking pattern, such as loitering [2–5] and following [6]. Based on a predefined tracking pattern, a tracking problem can be converted into a stabilization problem and then solved by conventional control methods. For instance, the loitering pattern guides a UAV to circle around a GMT with a given stand-off distance, and the resulting trajectory of the UAV expressed in the GMT's frame is a circle with a predefined radius. Consequently,

M. Zhang (✉) · H. H. T. Liu
Institute for Aerospace Studies, University of Toronto,
4925 Dufferin Street, Toronto, ON, M3H 5T6 Canada
e-mail: mingfeng.zhang@mail.utoronto.ca

H. H. T. Liu
e-mail: liu@utias.utoronto.ca

this tracking problem becomes a stabilization problem that seeks to regulate the position of a UAV on a moving circle, which is generally easier to solve. The so-called Lyapunov vector field (LVF) method and its variants were adopted by many researchers to formulate loitering-based tracking algorithms [2–5]. Dobrokhodov, Kaminer, and Jones also proposed a nonlinear control algorithm for a UAV to perform target loitering [7]. These loitering algorithms drive a UAV to fly along a circular path with respect to a GMT, which comprises a series of vantage points for the UAV to observe the GMT, so this pattern is generally desired for target monitoring [8]. However, these algorithms usually suffer from one critical limitation: they are only applicable to tracking tasks with a target that is much slower than the UAV. This is because these algorithms regulate both the separation distance and the circling angular velocity between the UAV and the GMT [3, 4, 9, 10]. The aforementioned maneuverability disparity between the two vehicles renders this requirement difficult to satisfy, especially when the GMT's speed varies over a large range. When the GMT's speed is smaller than the UAV's minimum speed, the UAV needs to circle around the GMT in order to keep the GMT within its proximity; however, when the GMT's speed is close to the UAV's, the UAV will lose tracking as a result of failing to maintain the predefined separation distance and the circling angular velocity simultaneously. To track fast-moving targets, researchers proposed the so-called "following" pattern, which guides a UAV to keep a GMT within a certain distance in front [6]. However, this pattern is only applicable to a GMT that moves faster than the UAV's minimum speed. Researchers recently proposed more comprehensive tracking algorithms that can accommodate targets with speeds varying over a large range. Oliveira and Encarnação developed a switching algorithm which consists of a following-based tracking law and a loitering-based tracking law [11]. This algorithm switches between the two patterns depending on the target speed and the relative distance, and it guarantees to keep the target in the vicinity of the UAV even if the target moves at a speed lower than the UAV's minimum speed. Fu, Feng, and Gao approached this problem by proposing a simple and effective algorithm which guides a fixed-wing UAV to track a GMT by following a sequence of heuristically constructed way-points [12]. These way-points are carefully calculated and recursively corrected according to the relative position and orientation between the UAV and the GMT in order to ensure visibility and minimize the UAV's turning rate. Since the GMT is independently controlled and its motion is usually hard to predict, the game theory was also applied to study this tracking problem in the framework of pursuit-evasion games [13, 14]. In addition, numerical methods, such as model predictive control, were also adopted to solve this problem with some success [15, 16]. These improved tracking algorithms were verified through numerical simulations and seemed to offer a promising solution to this problem, but the stability of these algorithms remains largely an open question.

In the meantime, the problem of target tracking using multiple UAVs was also extensively studied in the literature. It is mainly motivated by the benefits of multi-UAV cooperation, including expanded sensor coverage, enhanced detection capability, and increased system redundancy. These benefits are highly advantageous to the success of target tracking tasks, especially in the case of uncooperative or highly agile targets. To the best knowledge of the authors, the loitering pattern is the most popular pattern adopted in cooperative tracking algorithms. Some of the aforementioned loitering-based tracking algorithms involving a single UAV were extended to the multi-UAV scenario by including some motion coordination mechanisms [5]. These modifications are usually made to distribute multiple UAVs on a loitering circle with prescribed inter-vehicle angular separation, which can be designed to maximize the UAV team's visibility of a target and to improve the performance of target estimation. For example, evenly placing multiple UAVs on the loitering circle was found to be an optimal configuration to collect information of a given target using range [17] or bearing-only [18] sensors. Different strategies were applied to coordinate the motion of multiple UAVs in cooperative tracking [19], but they all impose additional requirements on the UAVs' maneuverability. In other words, the admissible range of the target's speed is further limited for given UAVs in the case of multi-UAV tracking. Simulation results given in [4] suggest that the target speed must be below 30 percent of the UAV's nominal speed. A numerical example given in [20] indicates that fixed-wing UAVs with maximum bank angle of 35 degrees, airspeed of 15 m/s, and desired orbit radius of 100 m can only track a target moving

under 5.17 m/s. In summary, in order to relax the limit of the GMT's speed range in the UAV-GMT tracking problem, it is imperative to develop more advanced tracking and cooperation strategies to address challenges stemmed from the maneuverability difference between these two types of vehicles.

This paper attempts to address this issue by proposing a new cooperative tracking scheme, which consists of a loitering algorithm and a formation algorithm. The proposed loitering algorithm significantly simplifies the tracking strategy and relaxes the admissible range of the GMT's speed. Based on sliding mode control, it is designed for a single UAV to perform target tracking, and it only regulates the separation distance between the UAV and the GMT. Because this strategy leaves the circling angular velocity as a free parameter, it allows the GMT's speed to vary up to the UAV's, while the UAV can maintain loitering by flying at a fixed speed. When the GMT's speed is small, the UAV circles around the GMT, and the circling angular velocity decreases as the GMT's speed increases. When the GMT's speed approaches the UAV's, the UAV's trajectory tends to be parallel to the GMT's, and the circling angular velocity approaches zero. The formation algorithm is proposed to enable multi-UAV cooperation in target tracking by keeping multiple fixed-wing UAVs flying in a circular formation with equal inter-vehicle angular separation. It is designed in a special way such that it does not affect the admissible range of the GMT's speed. In other words, when the proposed loitering algorithm is extended to the multi-UAV case, the admissible range of GMT's speed will remain unchanged if the UAVs' motion is coordinated by the proposed formation algorithm. The proposed formation algorithm is based on the virtual structure approach, and the resulting formation is a rigid equilateral polygon. The collective motion of the entire formation is solely represented by the formation center (i.e., the polygon center), which can be controlled independently to control the motion of the entire formation. In this work, the formation center is treated as a virtual UAV, and the aforementioned loitering algorithm is directly implemented on it. Under this two-layer tracking strategy, which is illustrated in Fig. 1, the placement of multiple UAVs relative to the target is fundamentally different from existing cooperative tracking algorithms. Existing algorithms are commonly designed to keep a moving target at the formation center to ensure continuous visibility

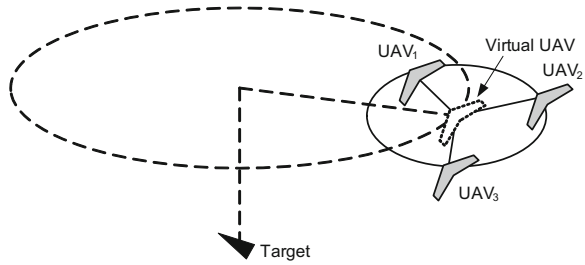

Fig. 1 Illustration of tracking a moving target by a formation of three UAVs. The virtual UAV, representing the collective motion of the three-UAV formation, is loitering around the target on the big, dashed circle centered at the target, while the three physical UAVs are flying in a equilateral triangle centered at the virtual UAV

or to improve estimation performance. By contrast, the proposed tracking strategy evenly distributes multiple UAVs on a circle centered at the virtual UAV, while the virtual UAV is controlled to stay on a circle centered at the moving target under the loitering algorithm. Further, the formation geometry is deliberately defined in an inertial frame, so the resulting motion of each UAV tends to be parallel to the virtual UAV once the desired formation is reached. In other words, the resulting polygon of the UAV formation does not rotate around the virtual UAV in perfect formation. Because of these two special arrangements, the proposed cooperative tracking algorithm does not cause additional requirements on the UAV's motion capability in order to maintain formation and tracking simultaneously. The physical UAVs only need to be slightly more maneuverable than the virtual UAV in order to be able to reach a desired formation from arbitrary initial positions and to reject external disturbances. Since the proposed loitering algorithm allows the GMT to be almost as fast as the UAV and the formation algorithm does not cause additional requirement on the UAV's motion capability, the two-layer strategy allows the cooperative tracking algorithm to accommodate a GMT moving almost as fast as the UAVs. Under this strategy, UAVs will cease to maintain a constant stand-off distance with respect to the GMT. In fact, the relative distance between the GMT and UAVs will be time-varying. Nevertheless, the formation geometry can be designed to ensure that at any instant of time one or more UAVs remain insider the loitering circle of the virtual UAV. In other words, continuous visibility of the target can be maintained by a properly designed formation geometry. In summary,

the key novelty of the proposed cooperative tracking scheme, including the loitering algorithm and the formation algorithm, lies in its capability of extending the admissible speed limit of the GMT to the speed of the UAV.

The rest of this paper is organized as follows. In Section 2, the kinematic model describing the relative motion between a UAV and a GMT is derived. The loitering algorithm based on sliding mode control as well as its stability proof is presented in Section 3, followed by the formation algorithm and its stability analysis in Section 4. In Section 5, the two algorithms are integrated and verified through numerical simulations, and they are compared with a loitering algorithm based on the LVF method. Some concluding remarks are provided in Section 6.

2 Problem Formulation

In this section, the kinematic models of a fixed-wing UAV and a GMT are presented, and the relative motion is derived.

2.1 Vehicle Models

The tracking problem studied in this work is considered in a planar environment since only the relative motion on the horizontal plane between a UAV and a GMT is of interest. The UAV is assumed to be equipped with a low-level flight control system which provides altitude-hold, speed-hold, and heading-hold capabilities [21]. This study only concerns about designing guidance commands (e.g., airspeed and turning rate) for this low-level controller to perform target tracking. The UAV's motion on the horizontal plane in the presence of environmental wind can be described by the following equations.

$$\begin{cases} \dot{x}_a &= v_a \cos\psi_a + v_w \cos\psi_w \\ \dot{y}_a &= v_a \sin\psi_a + v_w \sin\psi_w \\ \dot{v}_a &= u_a \\ \dot{\psi}_a &= \omega_a \end{cases} \tag{1}$$

where (x_a, y_a), v_a, and ψ_a denote the UAV's inertial position, airspeed, and heading angle, respectively; u_a and ω_a, denoting the UAV's acceleration and turning rate, are the control inputs; v_w and ψ_w denote the speed and direction of environmental wind. The airspeed of fixed-wing UAVs is constrained between two positive numbers. The lower bound is roughly imposed by the stall condition, and the upper bound is mainly determined by the thrust limit.

Small UAVs are inevitably subject to the disturbance of environmental wind, which could significantly affect the performance of UAV missions. A common practice in UAV applications is to directly control the ground speed and the course angle of UAVs partly because of the difficulty of estimating the velocity of environmental wind. Small UAVs have limited payload capacity, so onboard pressure sensors are usually of compromised quality and might not be able to provide reliable measurements of airspeed. On the other hand, compact and light GPS receivers are commonly installed on small UAVs and can obtain a UAV's motion parameters in an inertial frame; therefore, it is convenient to directly control a UAV's motion relative to the ground. However, this treatment relies on a high-gain low-level flight controller in order to reject the wind disturbance to the course angle, and the robustness of the resulting guidance system is essentially determined by the low-level flight controller. In this work, the loitering and formation algorithms control the UAV's airspeed and heading angle by feeding forward the wind velocity in control loops, thus allowing a low-gain flight controller to take care of the UAV's nonlinear dynamics.

The GMT's kinematics can also be described by equations similar to Eq. 1 by excluding the wind terms, with its position, heading angle, linear speed, acceleration, and turning rate denoted by (x_t, y_t), ψ_t, v_t, u_t, and ω_t, respectively. In this work, it is assumed that the UAV can sense its own states and estimate the wind along with the GMT's states.

2.2 Relative Motion Model

The relative motion between a fixed-wing UAV and a GMT in an inertial frame is illustrated in Fig. 2, and it can be described by

$$\dot{l} = v_a \sin\bar{\psi}_a - v_t \sin\bar{\psi}_t + v_w \sin\bar{\psi}_w \tag{2}$$

$$\dot{\lambda} = \frac{-v_a \cos\bar{\psi}_a + v_t \cos\bar{\psi}_t - v_w \cos\bar{\psi}_w}{l + R} \tag{3}$$

where $\bar{\psi}_* = \psi_* - \lambda$; R is a positive constant denoting the desired separation distance; l denotes the distance error; $\lambda = \theta - \pi/2$ with $\theta \in [0, 2\pi)$, and it is wrapped into the range $[0, 2\pi)$. This relative motion model permits a formulation to directly control the distance

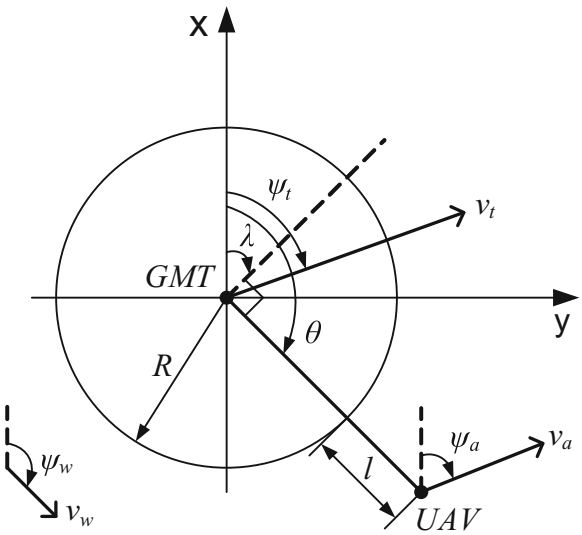

Fig. 2 Tracking a moving target by a UAV

between the UAV and the GMT. The angle λ defines the orientation of the line connecting the two vehicles. It is not directly controlled because the loitering-based tracking only concerns about the separation distance. The relative motion model suggests that the target motion and the wind can be consolidated and modeled as a single velocity vector; therefore, the target motion described in the following analysis can be treated as the combined velocity of the target and the environmental wind. The vehicle and wind speeds are assumed to satisfy $0 \leq v_t + v_w < v_a$ so that the tracking problem is feasible.

The control goal of this tracking problem is to regulate the distance error l to zero. For the single-UAV-single-GMT tracking problem, we assume the UAV speed is constant and only uses its turning rate ω_a as its control input. Constant speed flight is generally desired in practice because fixed-wing planes usually fly at their cruise speed for the sake of fuel efficiency. Besides, the speed of fixed-wing UAVs is constrained between two positive numbers, and it is theoretically challenging to deal with a control problem with this type of input constraints. To the best knowledge of the authors, only Ren and Beard explicitly considered the speed constraint of a fixed-wing UAV in a trajectory tracking problem [22]. Therefore, constant speed flight not only improves the fuel efficiency of the UAV, but also significantly simplifies the control problem. Furthermore, the resulting motion of the UAV under this treatment is much easier for the low-level flight controller to achieve.

3 Target Loitering Based on Sliding Model Control

The dynamics of the distance error l described by Eq. 2 indicates that l cannot be directly controlled by the UAV's turning rate ω_a. Instead, the UAV's heading angle ψ_a must be controlled to track a proper value that can gradually drive the distance error l to zero. This motives the usage of sliding mode control, in which a sliding manifold is defined to generate a proper trajectory for the heading angle to achieve the control goal. Once the heading angle is controlled to stay on the manifold using the UAV's turning rate ω_a, the distance error l will converge to zero. In this section, a loitering algorithm based on sliding mode control is presented, and it is further modified to eliminate chattering involved in sliding mode control.

3.1 Tracking Law

The steady value of $\bar{\psi}_a$, denoted by $\bar{\psi}_a^d$, can be computed by setting $\dot{l} = 0$ in Eq. 2. The steady state $\bar{\psi}_a^d$ is given by

$$\bar{\psi}_a^d = \sin^{-1}\left(\frac{v_t \sin\bar{\psi}_t - v_w \sin\bar{\psi}_w}{v_a}\right).$$

The condition $0 \leq v_t + v_w < v_a$ ensures that the steady state $\bar{\psi}_a^d$ in the foregoing equation is well defined with $\bar{\psi}_a^d \in (-\pi/2, \pi/2)$. Define $\tilde{\psi}_a = \bar{\psi}_a - \bar{\psi}_a^d$ and wrap it into the range $(-\pi, \pi]$, then the dynamics of the distance error can be expressed as

$$\begin{aligned}\dot{l} &= v_a \sin(\bar{\psi}_a^d + \tilde{\psi}_a) - v_t \sin\bar{\psi}_t + v_w \sin\bar{\psi}_w \\ &= v_a\Big(\sin\bar{\psi}_a^d(\cos\tilde{\psi}_a - 1) + \cos\bar{\psi}_a^d \sin\tilde{\psi}_a\Big). \end{aligned} \quad (4)$$

Substituting the trigonometric identities $\cos\tilde{\psi}_a = 1 - 2\sin^2(\tilde{\psi}_a/2)$ and $\sin\tilde{\psi}_a = 2\sin(\tilde{\psi}_a/2)\cos(\tilde{\psi}_a/2)$ into Eq. 4 yields

$$\begin{aligned}\dot{l} &= 2v_a \sin\frac{\tilde{\psi}_a}{2}\cos\left(\bar{\psi}_a^d + \frac{\tilde{\psi}_a}{2}\right) \\ &= 2v_a \sin\frac{\tilde{\psi}_a}{2}\cos\frac{\bar{\psi}_a^d + \tilde{\psi}_a}{2}. \end{aligned} \quad (5)$$

The straight line connecting the GMT and the UAV divides the horizontal plane into two regions. We assume the UAV keeps its heading angle towards one

region such that $\bar{\psi}_a$ remains in the range $[-\pi/2, \pi/2]$, as shown in Fig. 2. As a result, the inequality $\cos(\bar{\psi}_a^d/2 + \bar{\psi}_a/2) > 0$ is valid since $\bar{\psi}_a^d \in (-\pi/2, \pi/2)$ by definition. Subsequently, the tracking error l will converge to zero asymptotically if we take $\tilde{\psi}_a = -\phi(l)$, in which $\phi(l)$ is a continuous function such that $l \cdot \phi(l) > 0$ for all $l \neq 0$ and $\phi(l) = 0$ if and only if $l = 0$. In the following, we will apply sliding mode control to design a control law to achieve this goal. The sliding manifold is designed as

$$s = \tilde{\psi}_a + c_1 \tan^{-1}(c_2 l) \tag{6}$$

where c_1 and c_2 are two positive gains to be designed.

The idea is to design a control law that constrains the motion of the original system (2) and (3) on the manifold $s = 0$, which guarantees that l will converge to zero as time tends to infinity. To that end, the following control law is proposed.

$$\omega_a = \dot{\lambda} + \dot{\bar{\psi}}_a^d - \frac{c_1 c_2 \dot{l}}{1 + c_2^2 l^2} - c_3 \mathrm{sgn}(s) \tag{7}$$

where c_3 is a positive gain, and $\mathrm{sgn}(s)$ is the signum function given by

$$\mathrm{sgn}(s) = \begin{cases} 1 & \text{if } s > 0 \\ 0 & \text{if } s = 0 \\ -1 & \text{if } s < 0. \end{cases}$$

The main conclusion can be summarized in the following theorem.

Theorem 1 *Suppose that there exists a positive number $\eta \in [0, 1)$ such that $v_t \leq \eta v_a$ and the positive gain $c_1 \in (0, 1]$ satisfies $\sin^{-1}\eta \leq (1 - c_1)\pi/2$, then the state l of the system (2) and (3) converges to zero under the control law given in Eq. 7. Moreover, $l = 0$ is globally asymptotically stable.*

Proof The derivative of the sliding variable is

$$\dot{s} = \omega_a - \dot{\lambda} - \dot{\bar{\psi}}_a^d + \frac{c_1 c_2 \dot{l}}{1 + c_2^2 l^2}$$

which becomes the following differential equation under the control input given by Eq. 7

$$\dot{s} = -c_3 \mathrm{sgn}(s).$$

Consider a Lyapunov function candidate $V = s^2/2$, then we have

$$\dot{V} = -c_3 \mathrm{sgn}(s) s = -c_3 |s|. \tag{8}$$

Thus, $W \triangleq \sqrt{2V} = |s|$ satisfies the following differential equality

$$D^+ W = -c_3$$

where $D^+ W$ stands for the right-hand derivative [23] of the non-differentiable variable W. The solution is given by

$$W(s(t)) = W(s(0)) - c_3 t$$

which indicates that the trajectory will reach the manifold $s = 0$ in finite time, and moreover, it will remain on the manifold thereafter as shown by $\dot{V} = -c_3 |s|$.

On the manifold $s = 0$, the following equality can be derived from Eq. 6

$$\bar{\psi}_a = \bar{\psi}_a^d - c_1 \tan^{-1}(c_2 l).$$

Thus the inequality $\sin^{-1}\eta \leq (1 - c_1)\pi/2$ ensures that

$$\left|\bar{\psi}_a\right| \leq \left|\bar{\psi}_a^d\right| + \left|c_1 \tan^{-1}(c_2 l)\right| \leq \sin^{-1}\eta + c_1 \frac{\pi}{2} \leq \frac{\pi}{2}.$$

Note that the reaching phase, during which the sliding variable s approaches zero, is independent of $\bar{\psi}_a$, so $s = 0$ can always be reached in finite time regardless of the value of $\bar{\psi}_a$.

On the manifold $s = 0$, the distance error's dynamics given by Eq. 5 is reduced to

$$\dot{l} = -2 v_a \cos\frac{\bar{\psi}_a^d + \bar{\psi}_a}{2} \sin\frac{c_1 \tan^{-1}(c_2 l)}{2}$$

where $\cos(\bar{\psi}_a^d/2 + \bar{\psi}_a/2) > 0$ because $\bar{\psi}_a \in [-\pi/2, \pi/2]$ on the manifold and $\bar{\psi}_a^d \in (-\pi/2, \pi/2)$ by definition. Consequently, the foregoing equation ensures that the tracking error l converges to zero asymptotically, which can be proven with a Lyapunov function candidate $U = l^2/2$. □

Remark 1 The value of c_1 determines the admissible speed range of the GMT that can be tracked by a UAV with a given speed. The speed ratio η approaches one as c_1 approaches zero, implying that the UAV can maintain tracking of a target with a speed up to its speed by decreasing c_1. Besides, c_1 must satisfy $c_1 \leq 1$ as η cannot be negative. On the other hand, the tracking problem becomes infeasible if the GMT is as fast as or faster than the UAV; therefore, the admissible speed limit of the GMT is termed as "almost as fast as the UAV".

3.2 Chattering-Free Tracking Law

It is well known that the sliding mode control method suffers from chattering, which is mainly caused by imperfect switching devices and unmodeled delays. In order to eliminate chattering, the signum function can be replaced by a high-slope saturation function, which is defined as

$$\text{sat}(y) = \begin{cases} y & \text{if } |y| \le 1 \\ \text{sgn}(y) & \text{if } |y| > 1. \end{cases}$$

Subsequently, the modified control law becomes

$$\omega_a = \dot{\lambda} + \dot{\bar{\psi}}_a^d - \frac{c_1 c_2 \dot{l}}{1 + c_2^2 l^2} - c_3 \text{sat}\left(\frac{s}{\epsilon}\right) \tag{9}$$

where ϵ is a positive constant to be designed. The parameter ϵ affects the algorithm's performance in eliminating chattering. A small value for ϵ is desired for better accuracy, but a too small value is likely to induce chattering in the presence of delays or unmodeled dynamics. Its value should be determined in practice through trial and error by considering the chattering-inducing characteristics of the devices used to implement the algorithm. A modified sliding mode control law with a saturation component can generally achieve ultimate boundedness with a bound that can be reduced by decreasing ϵ; that is, the modified control law will stabilize the system at a new equilibrium point, resulting in a steady-state error. However, if the gains are chosen properly, the modified control law given by Eq. 9 can retain asymptotic stability for the original system. This is summarized in the following theorem.

Theorem 2 *Suppose that there exists a positive number $\eta \in [0, 1)$ such that $v_t \le \eta v_a$, the positive gain $c_1 \in (0, 1]$ satisfies $\sin^{-1}\eta \le (1 - c_1)\pi/2$, and the positive constant ϵ satisfies $\epsilon/c_1 \le \pi/2$. Then, the state l of the system (2) and (3) converges to zero under the control law given in Eq. 9. Moreover, $l = 0$ is globally asymptotically stable.*

Proof When $|s| \ge \epsilon$, the control law (9) is the same as the original sliding mode control law (7), and hence the equality given in Eq. 8 remains valid. Therefore, whenever $|s(0)| > \epsilon$, $|s(t)|$ will be strictly decreasing until it reaches the set $\{|s| \le \epsilon\}$ in finite time and remains inside thereafter. We can derive from Eq. 6 that $\tilde{\psi}_a = s - c_1 \tan^{-1}(c_2 l)$ and hence $\left|\tilde{\psi}_a\right| \le \epsilon + c_1 \pi/2 \le \pi$ because $\epsilon/c_1 \le \pi/2$ and $c_1 \in (0, 1]$. Then, the dynamics of l inside $\{|s| \le \epsilon\}$ becomes

$$\dot{l} = 2v_a \cos\frac{\bar{\psi}_a^d + \bar{\psi}_a}{2} \sin\frac{s - c_1 \tan^{-1}(c_2 l)}{2}.$$

The derivative of $U = l^2/2$ satisfies

$$\forall\, |l| > \frac{1}{c_2}\tan\frac{\epsilon}{c_1},$$
$$\dot{U} = -2v_a \cos\frac{\bar{\psi}_a^d + \bar{\psi}_a}{2} \sin\frac{c_1 \tan^{-1}(c_2 l) - s}{2} l < 0.$$

Thus, the modified control law (9) drives the original system to the set $\Omega_\epsilon = \{|l| \le \frac{1}{c_2}\tan\frac{\epsilon}{c_1},\ \{|s| \le \epsilon\}\}$ in finite time and confines it inside thereafter.

Inside Ω_ϵ, the saturation component in Eq. 9 is reduced to $-c_3 s/\epsilon$, and then the closed-loop system can be expressed as

$$\begin{cases} \dot{\tilde{\psi}}_a &= -a \sin\frac{\tilde{\psi}_a}{2} - \frac{c_3}{\epsilon} s \\ \dot{s} &= -\frac{c_3}{\epsilon} s \end{cases}$$

where a is defined as

$$a = \frac{2c_1 c_2 v_a}{1 + c_2^2 l^2} \cos\frac{\bar{\psi}_a^d + \bar{\psi}_a}{2}.$$

Note that a is a time-varying but positive variable. Inside Ω_ϵ, the minimum value of a is found to be

$$a_{\min} = \frac{2c_1 c_2 v_a}{1 + \tan^2\frac{\epsilon}{c_1}} \cos\frac{\sin^{-1}\eta + \pi/2}{2}.$$

Considering a Lyapunov function candidate $V_1 = 4\sin^2(\tilde{\psi}_a/4) + \beta s^2/2$ for the closed-loop system within Ω_ϵ with $\beta > c_3/(4\epsilon a_{\min})$, it can be found that

$$\dot{V}_1 = -\beta\frac{c_3}{\epsilon}\left(s + \frac{1}{2\beta}\sin\frac{\tilde{\psi}_a}{2}\right)^2 - \left(a - \frac{c_3}{4\beta\epsilon}\right)\sin^2\frac{\tilde{\psi}_a}{2}$$

which is negative definite. Therefore, within Ω_ϵ, both $\tilde{\psi}_a$ and s will converge to zero asymptotically as time tends to infinity under the control law (9). From Eq. 6, it can be concluded that l also converges to zero asymptotically. □

4 Cooperative Tracking Through Formation Flight

The tracking algorithm presented in the preceding section enables target loitering using a single UAV. A

single UAV is sufficient for the tracking task, provided that the target states are available. If the target states are not provided and must be estimated by the UAV, a single UAV might be insufficient because of its limitation in the estimation task. The sensing coverage of a single UAV is usually limited, and the observation capability of a single UAV may be restricted by the observability issue of some types of sensors. One example is vision sensors, such as monocular cameras, which are are widely used as the primary observation sensor for small UAVs because they suit the stringent payload limitation of small UAVs. Monocular cameras only provide bearing-only measurements and do not contain the range information of targets. The cooperation of multiple UAVs can overcome these issues. The range information and thus the full state of a moving target can be recovered by fusing visual measurements obtained by multiple vision-enabled UAVs based on the triangulation principle [18, 24, 25]. Besides, multiple UAVs in a formation can form an expanded sensor converge. Therefore, multiple UAVs, each with a limited sensor converge, can perform persistent tracking cooperatively in a formation, although the limited sensor converge may preclude them from performing this task individually. Further, multiple UAVs can carry different types of sensors that could complement each other, thus enhancing the overall observation performance [26]. In addition, a tracking system using multiple UAVs has a higher level of redundancy and hence is more reliable against vehicle failures.

Together with the proposed loitering algorithm, the formation algorithm developed in this section enables cooperative tracking using multiple UAVs. The proposed loitering algorithm only uses the UAV's turning rate as the control input; however, it is physically infeasible for multiple UAVs to simultaneously perform target loitering and maintain formation by solely varying their turning rates. In the literature, cooperative tracking algorithms need to vary either UAV speeds or loitering variables (e.g., loitering radius and inter-vehicle angular separation), in addition to the UAV turning rates [3–5, 20]. The proposed formation algorithm uses both turning rate and speed as control inputs, but it will be shown that UAVs only need to vary their speeds mildly in the process of reaching a desired formation. Once the desired formation is achieved, UAVs can move at a constant speed to perform target loitering and may only need to vary their speeds slightly in the presence of external disturbances.

4.1 Formation Geometry

Consider N fixed-wing UAVs of identical dynamics in the formation problem, and assume that all UAVs are flying at a fixed altitude, then the planar motion of the ith $(i = 1, 2, ..., N)$ UAV, denoted as UAV_i, can be described by the following unicycle model

$$\begin{cases} \dot{x}_i &= v_i \cos\psi_i \\ \dot{y}_i &= v_i \sin\psi_i \\ \dot{v}_i &= u_i \\ \dot{\psi}_i &= \omega_i \end{cases} \quad (i = 1, 2, ..., N) \tag{10}$$

where (x_i, y_i), v_i, and ψ_i denote UAV_i's inertial position, airspeed, and heading angle, respectively; u_i and ω_i, denoting UAV_i's acceleration and turning rate, are the control inputs.

In this work, the UAV team is required to maintain a circular formation with equal inter-vehicle angular separation. The resulting formation is a rigid equilateral polygon, and its center represents the motion of the entire formation. The polygon center can be regarded as a virtual leader of the UAV team. In this work, this virtual UAV leader, denoted as UAV_0, is described by Eq. 10 as well, and its acceleration, airspeed, and turning rate are denoted by u_0, v_0, and ω_0,

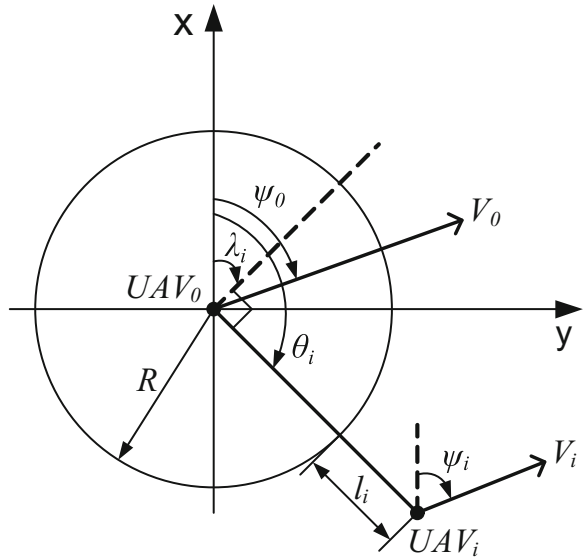

Fig. 3 Geometry of virtual structure formation in an inertial frame

respectively. The motion of the UAV team as a rigid formation can be controlled by specifying u_0 and ω_0 for a designated mission, such as target loitering.

The geometry between UAV_0 and UAV_i in the formation is depicted in Fig. 3. Assuming that all UAVs, including the virtual UAV, are subject to the same wind disturbance, the relative motion between UAV_0 and UAV_i can be express as

$$\begin{aligned}\dot{l}_i &= v_i \sin(\psi_i - \lambda_i) - v_0 \sin(\psi_0 - \lambda_i)\\ \dot{\lambda}_i &= \frac{-v_i \cos(\psi_i - \lambda_i) + v_0 \cos(\psi_0 - \lambda_i)}{l_i + R}\end{aligned}$$

where $\lambda_i = \theta_i - \pi/2$ and $\theta_i \in [0, 2\pi)$.

In this work, it is assumed that each UAV can sense its states and has the state information of the virtual UAV. The virtual UAV can be maintained by one UAV within the group and broadcast to the rest of the group. It can also be maintained by a ground station and transmitted to the UAV group. The variables λ_i $(i = 1, 2, ..., N)$ need to be exchanged among UAV individuals in order to achieve equal inter-vehicle angular separation. It will be shown shortly that they can be communicated locally, thus allowing a partially distributed implementation of the formation control algorithm. In this work, we assume that the graph of the UAV communication network is undirected and static, meaning the communication between two UAVs is bilateral and the communication topology is time-invariant.

Given the description of the formation requirement, the formation task can be summarized as follows

Problem 1 Consider N homogeneous fixed-wing UAVs with kinematics (10), design control laws u_i and ω_i $(i = 1, 2, ..., N)$ such that

1. $l_i \to 0$ as $t \to \infty$,
2. $(\lambda_{i+1} - \lambda_i) \to 2\pi/N$ as $t \to \infty$ $(\lambda_{N+1} = \lambda_1 + 2\pi)$.

4.2 Formation Control Law

In order to derive a control law for the UAV team to achieve the desired formation, consider the following Lyapunov function candidate, which consists of four components.

$$V = V_1 + V_2 + V_3 + V_4. \tag{11}$$

The Lyapunov function components are defined as

$$V_1 = \frac{k_1}{2}\sum_{i=1}^{N} l_i^2 \qquad V_2 = \frac{k_2}{2}\bar{\boldsymbol{\lambda}}^T \mathbf{L}\bar{\boldsymbol{\lambda}}$$

$$V_3 = \frac{k_3}{2}\sum_{i=1}^{N} \tilde{v}_i^2 \qquad V_4 = \frac{k_4}{2}\sum_{i=1}^{N} \tilde{\psi}_i^2$$

where $\bar{\boldsymbol{\lambda}} = [\bar{\lambda}_1\ \bar{\lambda}_2\ \cdots\ \bar{\lambda}_N]^T$ with $\bar{\lambda}_i \triangleq \lambda_i - \frac{2i}{N}\pi$, $\tilde{v}_i \triangleq v_i - v_0$, and $\tilde{\psi}_i \triangleq (\psi_i - \psi_0) \in (-\pi, \pi]$; the matrix $\mathbf{L}$ is known as the graph Laplacian matrix of the UAV communication network, and it is symmetrical for an undirected graph [27]; parameters k_j $(j = 1, 2, 3, 4)$ are four positive constants to be designed. Note that $\tilde{\psi}_i$ is wrapped into the range $(-\pi, \pi]$.

The Lyapunov function components V_1, V_3, and V_4 are terms that regulate the distance, airspeed, and heading errors, respectively, while V_2 is the so-called coupling term that regulates the angular separation between UAV individuals. Differentiating the Lyapunov function components with respect to time yields

$$\begin{aligned}\dot{V}_1 &= k_1 \sum_{i=1}^{N} l_i\big(v_i \sin(\psi_i - \lambda_i) - v_0 \sin(\psi_0 - \lambda_i)\big)\\ &= k_1 \sum_{i=1}^{N} l_i\Big(\tilde{v}_i \sin(\psi_i - \lambda_i) + v_0 \cos(\psi_0 - \lambda_i)\sin\tilde{\psi}_i\\ &\quad + v_0 \sin(\psi_0 - \lambda_i)(\cos\tilde{\psi}_i - 1)\Big),\end{aligned}$$

$$\dot{V}_2 = k_2 \sum_{i=1}^{N} a_i \dot{\bar{\lambda}}_i$$

where $[a_1\ a_2\ \cdots\ a_N] \triangleq \bar{\boldsymbol{\lambda}}^T \mathbf{L}$ and

$$\begin{aligned}\dot{\bar{\lambda}}_i &= \frac{-v_i \cos(\psi_i - \lambda_i) + v_0 \cos(\psi_0 - \lambda_i)}{l_i + R}\\ &= \frac{1}{l_i + R}\Big(-\tilde{v}_i \cos(\psi_i - \lambda_i) + v_0 \sin(\psi_0 - \lambda_i)\sin\tilde{\psi}_i\\ &\quad + v_0 \cos(\psi_0 - \lambda_i)(1 - \cos\tilde{\psi}_i)\Big),\end{aligned}$$

$$\dot{V}_3 = k_3 \sum_{i=1}^{N} \tilde{v}_i (u_i - u_0), \qquad \dot{V}_4 = k_4 \sum_{i=1}^{N} \tilde{\psi}_i (\omega_i - \omega_0).$$

The control inputs for UAV$_i$ are defined as

$$u_i = u_0 - \phi_v(\tilde{v}_i) - \frac{1}{k_3}\Big(k_1 l_i \sin(\psi_i - \lambda_i) - \frac{k_2 a_i}{l_i + R}\cos(\psi_i - \lambda_i)\Big), \quad (12)$$

$$\begin{aligned}\omega_i = \omega_0 - \phi_\omega(\tilde{\psi}_i) - \frac{1}{k_4\tilde{\psi}_i}\Big(&k_1 l_i v_0 \cos(\psi_0 - \lambda_i)\sin\tilde{\psi}_i \\ &+ k_1 l_i v_0 \sin(\psi_0 - \lambda_i)(\cos\tilde{\psi}_i - 1) \\ &+ \frac{k_2 a_i}{l_i + R} v_0 \sin(\psi_0 - \lambda_i)\sin\tilde{\psi}_i \\ &+ \frac{k_2 a_i}{l_i + R} v_0 \cos(\psi_0 - \lambda_i)(1 - \cos\tilde{\psi}_i)\Big) \end{aligned} \quad (13)$$

where $\phi_v(\cdot)$ and $\phi_\omega(\cdot)$ are uniformly continuous functions to be designed. They satisfy $x \cdot \phi_v(x) \geq 0$ and $x \cdot \phi_\omega(x) \geq 0$, and $\phi_v(x) = \phi_\omega(x) = 0$ if and only if $x = 0$. When $\tilde{\psi}_i = 0$, the values of $(\sin\tilde{\psi}_i)/\tilde{\psi}_i$ and $(1 - \cos\tilde{\psi}_i)/\tilde{\psi}_i$ are found by taking their limits with $\tilde{\psi}_i$ approaching zero. It is found that $(\sin\tilde{\psi}_i)/\tilde{\psi}_i = 1$ and $(1 - \cos\tilde{\psi}_i)/\tilde{\psi}_i = 0$ when $\tilde{\psi}_i = 0$. Hence, the control input ω_i is well defined for $\tilde{\psi}_i \in (-\pi, \pi]$.

Substituting u_i and ω_i into Eq. 11 with positive gains k_1, k_2, k_3 and k_4 leads to

$$\dot{V} = -k_3 \sum_{i=1}^{N} \phi_v(\tilde{v}_i)\tilde{v}_i - k_4 \sum_{i=1}^{N} \phi_\omega(\tilde{\psi}_i)\tilde{\psi}_i.$$

Given the definition of V and the fact that $\dot{V} \leq 0$, it follows that the Lyapunov function candidate V and the errors $\tilde{v}_i$ and $\tilde{\psi}_i$ are bounded. It is trivial to verify that $\dot{V}$ is uniformly continuous. This, in conjunction with the boundedness of V, implies that $\dot{V}$ and subsequently $\tilde{v}_i$ and $\tilde{\psi}_i$ are all tending to zero according to Barbalat's lemma [23]. We can further verify that $\dot{\tilde{v}}_i$ and $\dot{\tilde{\psi}}_i$ are uniformly continuous. Hence, the boundedness of $\tilde{v}_i$ and $\tilde{\psi}_i$ implies that $\dot{\tilde{v}}_i$ and $\dot{\tilde{\psi}}_i$ tend to zero as well according to Barbalat's lemma [23], which leads to the conclusion that l_i and a_i tend to zero.

Table 1 Gains and parameters in the target loitering algorithm

c_1	c_2	c_3	ϵ
0.2	0.05	0.005	0.2

The main result of the formation control algorithm can then be summarized in the following theorem.

Theorem 3 *Consider N homogeneous fixed-wing UAVs with kinematics described by Eq. 10, given the control law described by Eqs. 12 and 13, the first requirement listed in Problem 1 is satisfied. Further, when the undirected graph of the UAV communication network is connected, the second requirement is also satisfied.*

Proof It has been shown both l_i and a_i ($i = 1, 2, ..., N$) converge to zero under the control law given by Eqs. 12 and 13. It is only left to prove that the

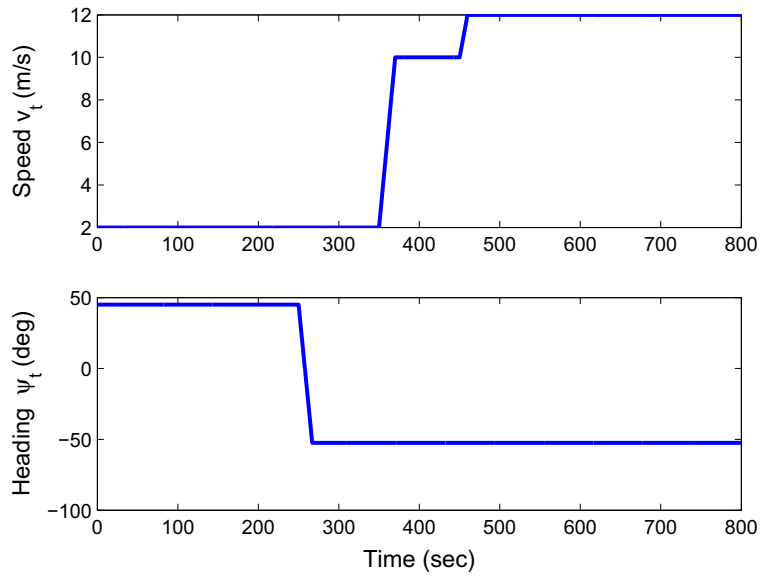

Fig. 4 GMT speed and heading angle

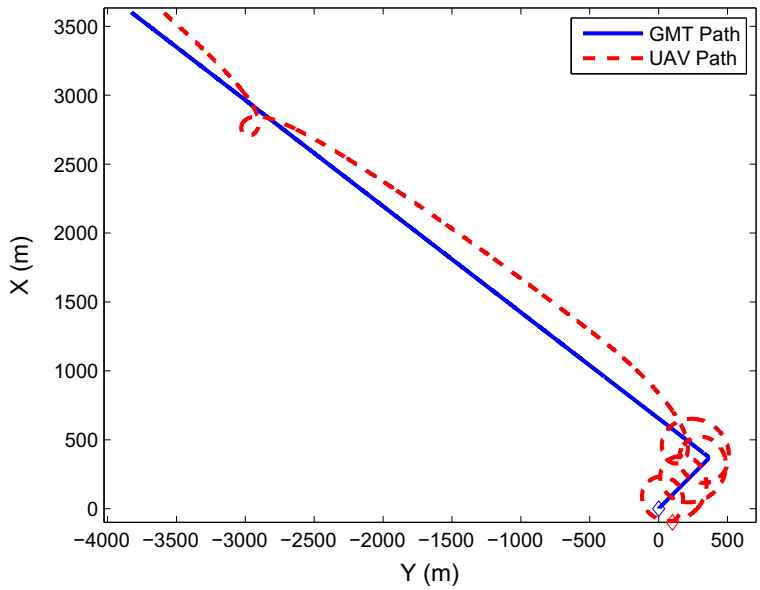

Fig. 5 UAV and GMT 2D trajectories in an inertial frame. Diamond markers are UAV and GMT starting positions

UAV team can reach equal inter-vehicle angular separation when the undirected graph of the UAV network is connected.

When the undirected graph of the UAV communication network is connected, the graph Laplacian matrix $\mathbf{L}$ is positive semi-definite, and the only solution to the equation $\mathbf{Lx} = 0$ is $\mathbf{x} = \alpha\mathbf{1}$. The vector $\mathbf{1} \in \mathbb{R}^N$ stands for a vector with all its entries as 1, and $\alpha = \sum_{i=1}^{N} x_i(0)/N$ [27]. Therefore, the condition $a_i = 0$ (i.e., $\mathbf{L}\tilde{\lambda} = 0$) implies that

$$\lambda_i - \frac{2i}{N}\pi = \frac{1}{N}\sum_{k=1}^{N}\left(\lambda_k(0) - \frac{2k}{N}\pi\right), \quad (i = 1, 2, ..., N).$$

Thus it can be concluded that

$$\lambda_j - \lambda_i = \frac{2(j-i)}{N}\pi, \quad (i, j = 1, 2, ..., N)$$

which satisfies the second requirement. □

Although the control laws (12) and (13) do not explicitly consider constraints on the UAV's speed, turning rate, and acceleration, they are designed to alleviate these constraints to some degree. For example, the first two terms in Eq. 12 tend to keep v_i close to v_0, so the UAVs' forward motion is sustained if v_0 is near the cruise speed of a physical UAV. The first two terms in Eq. 13 tend to keep ω_i close to ω_0. As the UAV team reaches the desired formation, v_i and ω_i $(i = 1, 2, ..., N)$ would respectively converge to v_0 and ω_0, indicating that the motion of UAV individuals tends to be parallel to the virtual UAV. This means the motion of UAV individuals is largely determined by the motion of the virtual UAV in perfect formation. In practice, the control effort of UAV individuals will be slightly different from that of the virtual UAV because of external disturbances and system uncertainties. Nevertheless, they will remain fairly close, and therefore the constraints on the UAV's speed and turning rate can be mitigated by properly setting the virtual UAV's speed and turning rate. If the initial placement of UAV individuals is far from the desired formation, UAV individuals may have to maneuver more than the virtual UAV in order to achieve the desired formation. In this scenario, gains k_i $(i = 1, 2, 3, 4)$ can be carefully tuned to avoid violating the UAVs' kinematic constraints. Further, hard constraints can be enforced as a last resort to ensure the UAVs' safety.

5 Simulation Results

In this section, the proposed tracking and formation algorithms are verified in two sets of numerical simulations. The first simulation case applies the chattering-free loitering algorithm for a single UAV to track a GMT. The second case integrates the loitering algorithm and the formation algorithm and applies them to a three-UAV fleet in the same tracking task. The two algorithms are also compared with a loitering algorithm based on the LVF method to

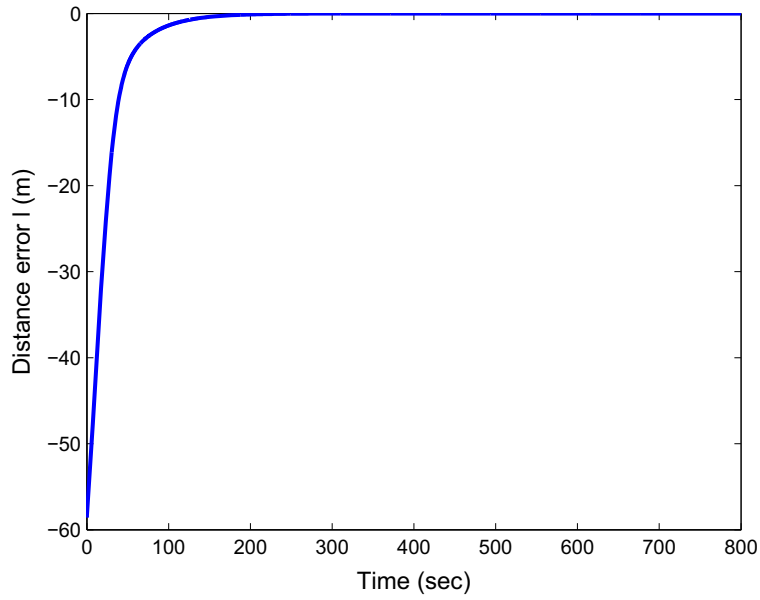

(a) Distance error

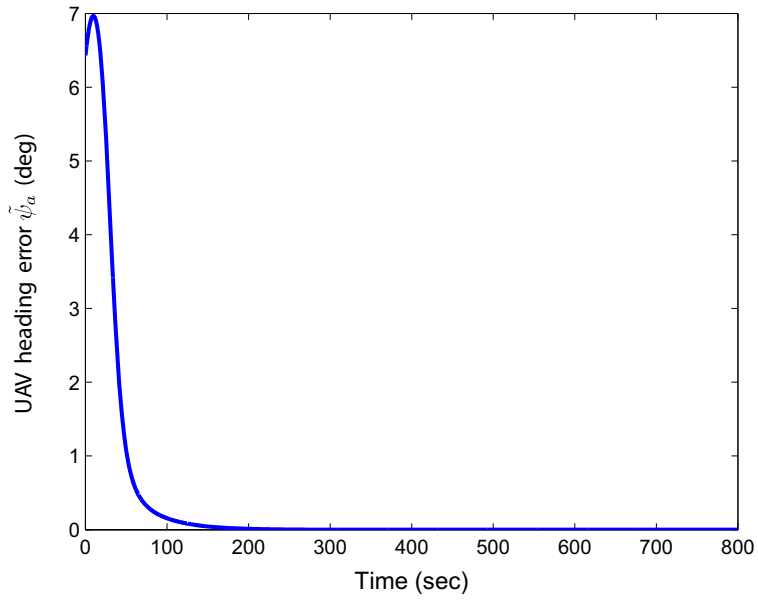

(b) UAV heading error

Fig. 6 The relative distance error and the UAV heading angle error

demonstrate their capability of tracking fast-moving targets.

The GMT's motion profile, including its speed and heading angle, is illustrated in Fig. 4, and it is used in both simulation cases and the comparative study. The GMT's speed, varying over a rather large range, starts at 2 m/s and accelerates to 10 m/s during 350-370 seconds and to 12 m/s during 450–460 seconds. The GMT's initial heading angle is 45 degrees, and it makes a sharp left turn of 97.4 degrees during 250-267 seconds. The target motion prescribed here should be regarded as the consolidated velocity of the GMT and the environmental wind. The gains and parameters used in the loitering algorithm are given in

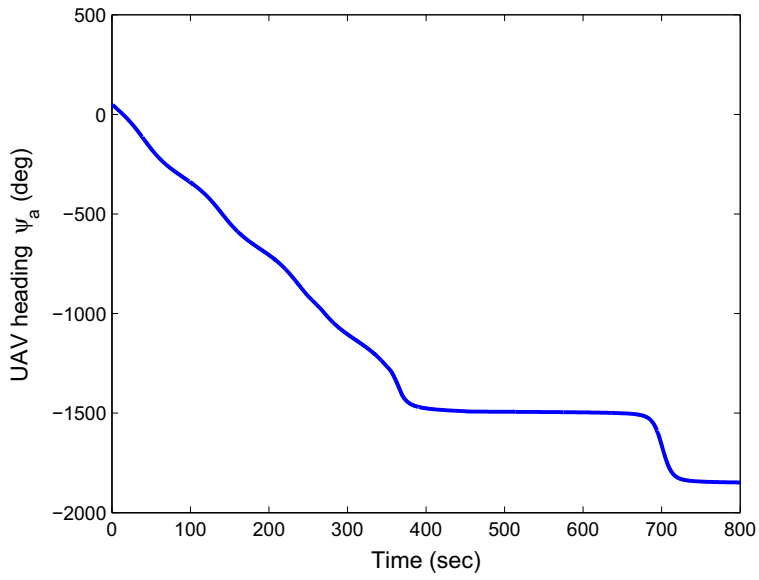

(a) UAV heading angle (unwrapped)

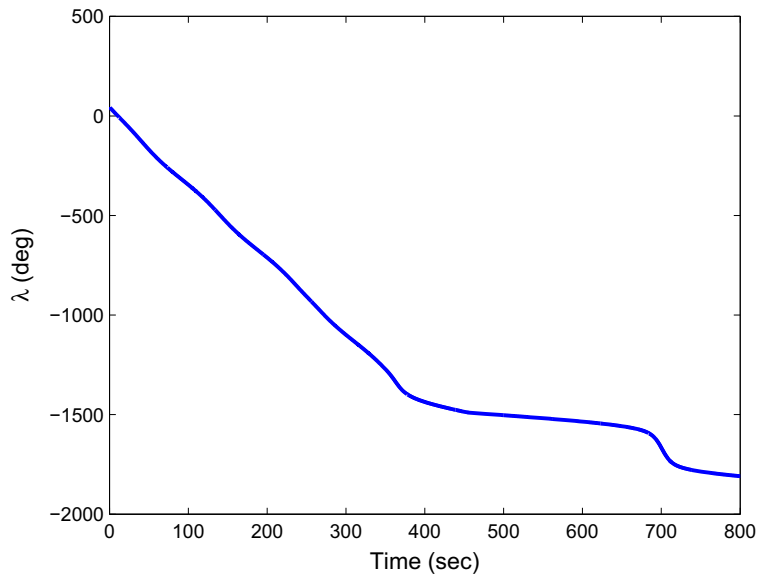

(b) Angle λ (unwrapped)

Fig. 7 UAV heading angle and angle λ. Both are unwrapped to produce smooth phase plots

Table 1. The gain $c_1 = 0.2$ leads to $\eta \leq 0.95$, indicating the UAV is able to track a target with its speed up to 95 percent of the UAV's speed. The values of c_2 and c_3 affect the converging speed of the loitering algorithms and the control effort (i.e., turning rate) of the UAV during the converging period. They are found mainly through a trial and error process.

5.1 Tracking a GMT Using a Single UAV

In the single-UAV-single-GMT tracking task, the desired separation distance between the GMT and the UAV is set as 200 m, which is a configuration successfully validated in real flight tests of similar UAV-GMT tracking algorithms [7]. The UAV's speed is fixed at

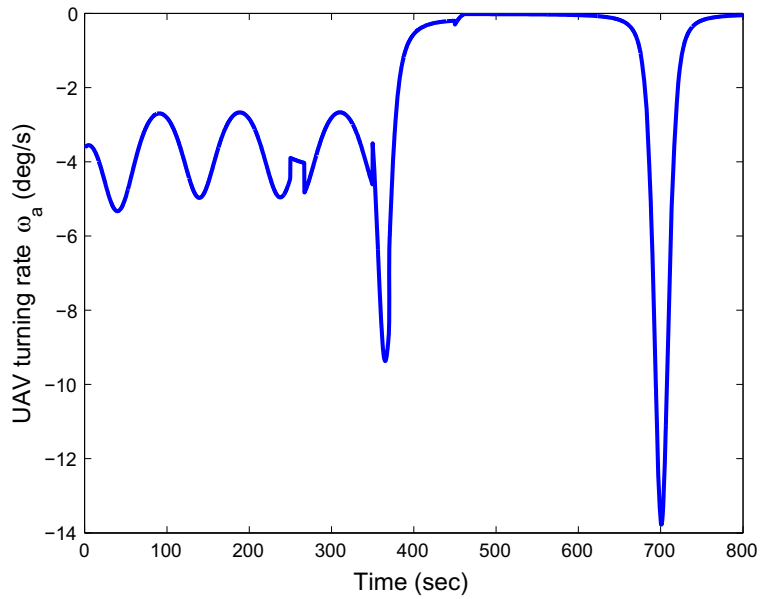

Fig. 8 UAV turning rate

13 m/s, and its initial position and heading angle are (−100, 100) m and 51.4 degrees.

The trajectories of the UAV and the GMT in the tracking mission are shown in Fig. 5. As we can see, the UAV is able to maintain a persistent circular motion around the GMT at the desired separation distance, while the actual speed ratio between them varies from 0.153 to 0.923. This clearly confirms that the proposed loitering algorithm is capable of tracking a target with a speed varying in a large range. From the distance error and heading angle error history illustrated in Fig. 6, we can observe that it takes about 200 seconds for the UAV to achieve the desired loitering pattern. The UAV's heading angle and the angle λ are presented in Fig. 7, and they demonstrate that the circular angular velocity approaches zero during the period when the UAV and GMT speeds are comparable. The UAV's control input, which is its turning rate, is shown in Fig. 8. It contains a few abrupt changes, which are caused by the speed and heading changes of

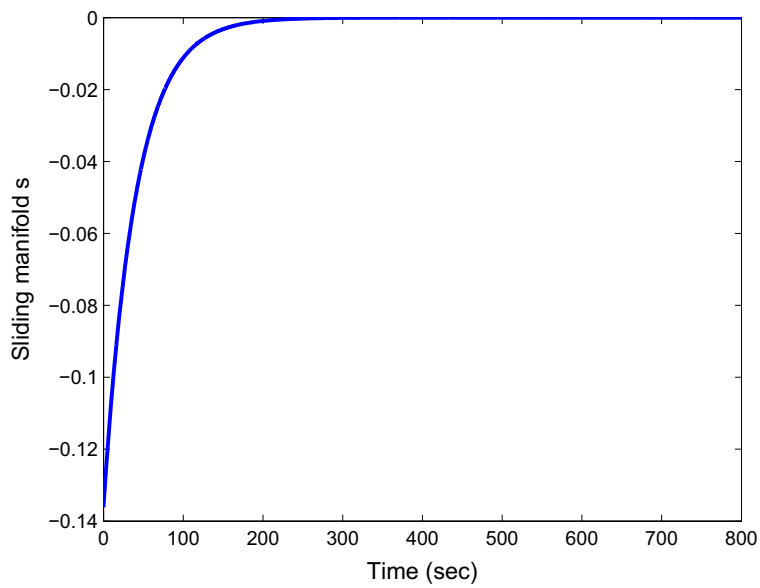

Fig. 9 The sliding manifold variable

Table 2 Gains of the formation control algorithm

k_1	k_2	k_3	k_4	k_v	k_ω
0.65	1950	10	250	1.8	0.0955

the GMT. The maximum turning rate in the simulation reaches 13.8 deg/s, and the UAV needs to maintain a bank angle around 10.3 degrees in order to achieve this turning rate under the coordinated-turn assumption. This bank angle is within a reasonable range for small fixed-wing UAVs. The sliding manifold variable, shown in Fig. 9, demonstrates that the modified tracking law is effective in eliminating the chattering phenomenon.

5.2 Cooperative Tracking Using Multiple UAVs

The second simulation integrates the loitering algorithm and the formation algorithm to perform cooperative tracking using three UAVs. This three-UAV fleet is required to maintain an equilateral triangular formation while tracking a GMT. The radius of the formation circle is 150 m, and the desired distance between the GMT and the formation center is set as 200 m. The chattering-free loitering algorithm is directly implemented on the virtual UAV of the formation; that is, $u_0 = 0$, $v_0 = 13$ m/s, and ω_0 is given by Eq. 9. The target tracking task is engaged at 150 seconds to allow a period for the UAV team to reach the desired formation. The GMT starts at $(586.90, 2057.68)$ m with a heading angle of 45 degrees, and its motion is described by Fig. 4 as well. The gains of the formation algorithm, found through a trial and error process, are given in Table 2. A hard constraint of 20 deg/s is enforced on the UAVs' turning rates.

The simulation results are presented in Figs. 10, 11, 12, 13, 14, 15 and 16. The trajectories of the three UAVs in the first 250 seconds are shown in Fig. 10, and the distance errors and the angular separation are shown in Fig. 14. They indicate that the desired formation is reached by the end of 220 seconds. The complete trajectories of the UAVs and the GMT throughout the simulation are plotted in Fig. 11. As we can see, both formation maintaining and target loitering tasks are successfully achieved despite the fact that the loitering task is engaged before the perfect formation is reached. All UAVs take a full turn during 577-745 seconds in order to maintain tracking. The trajectory segments during this period are highlighted within the box in Fig. 11, and they are zoomed in and replotted in Fig. 12. As we can see, the trajectories of all UAV individuals are parallel to each other during this period. This can be further confirmed by the UAVs' speeds and heading angles shown in Fig. 13. As we can see, the motion of all UAVs tends to be uniform. This indicates that all UAVs fly with the same speed and the same turning rate once the desired formation is achieved, regardless of the task assigned to the UAV team. The distance between the GMT and

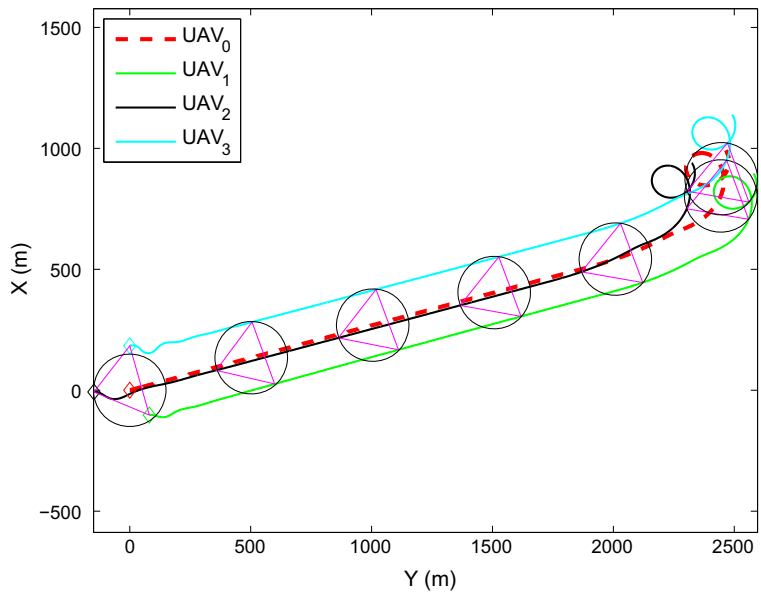

Fig. 10 UAV trajectories in reaching formation (0-250 sec). The triangles connect the three UAVs at the same time instants

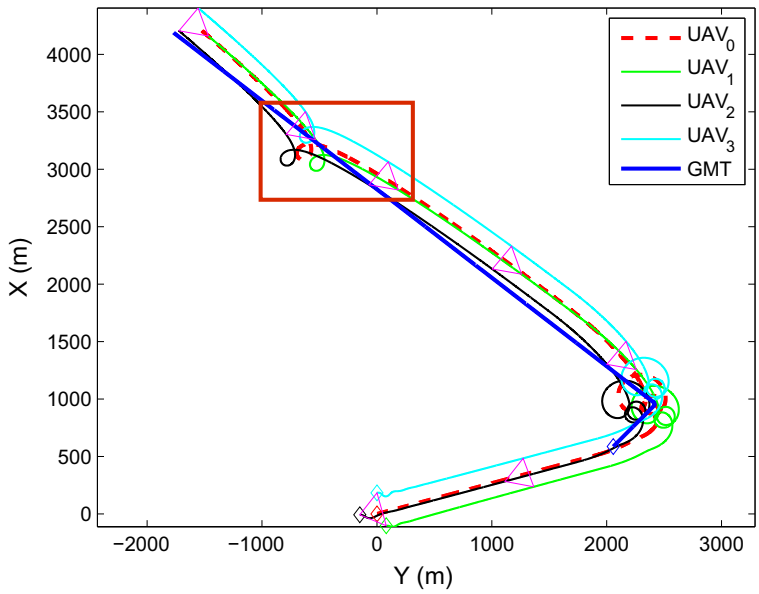

Fig. 11 UAV trajectories in cooperative tracking. The triangles connect the three UAVs at the same time instants. The box contains trajectories during 577–745 seconds, which are zoomed in Fig. 12

UAV individuals is shown in Fig. 15a, and the distance to the closest UAV and the distance between the GMT and the formation center are depicted in Fig. 15b. As we can see, at any instant of time after the initial period there is as least one UAV within 180.2 m from the GMT, which is below the desired separation distance, and the UAVs can briefly stay under 50 m from the GMT. The maximum distance is close to 350 m, indicating the detection radius of the UAVs must be greater than 350 m if the GMT needs to be seen by all three UAVs simultaneously. As shown in Fig. 16, the turning rates of the UAVs reach the hard constraint at 20 deg/s during the initial stage when the UAVs are maneuvering in order to reach the desired formation. However, the desired formation is successfully reached despite the hard constraint. In

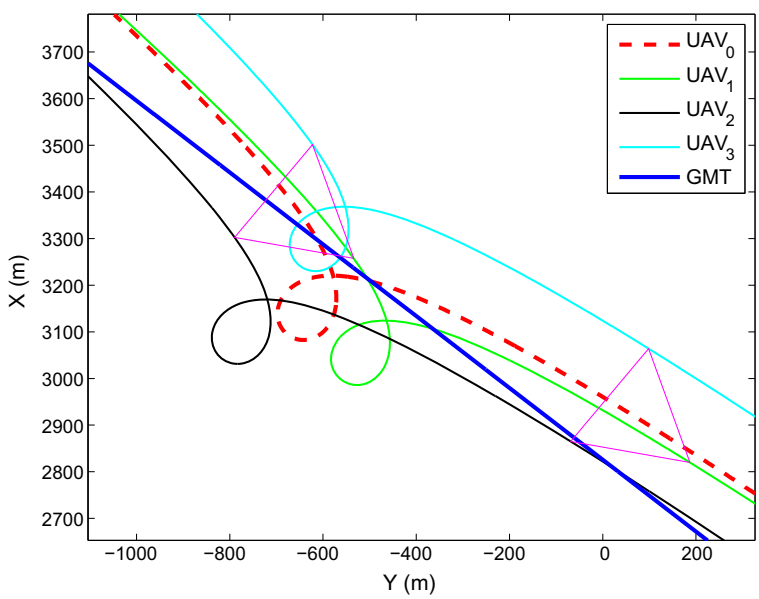

Fig. 12 UAV trajectories in maintaining formation (577-745 sec). The triangles connect the three UAVs at the same time instants

Fig. 13 UAV speeds and headings in reaching formation

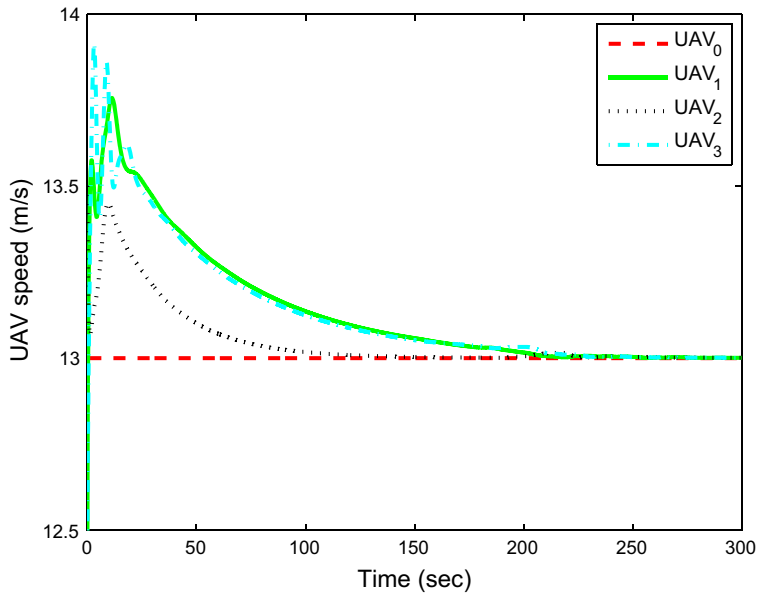

(a) Speed (0-300 sec)

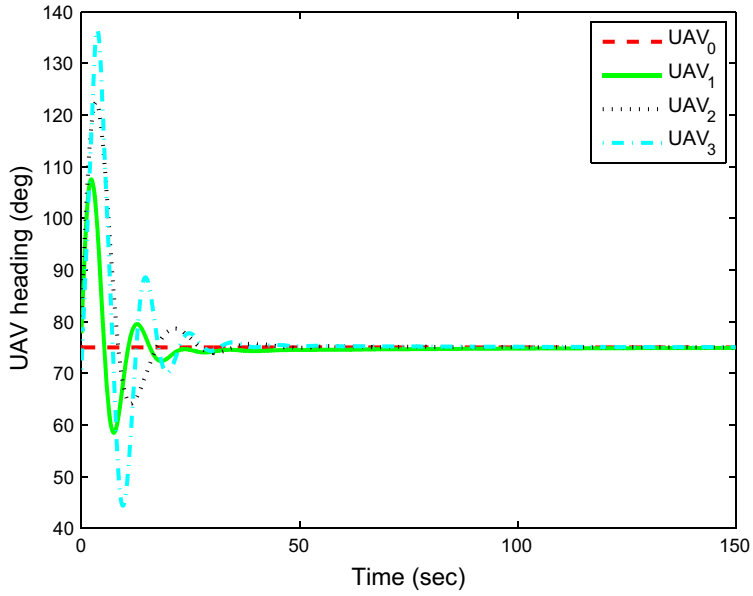

(b) Heading (0-150 sec)

practice, a more stringent constraint can be enforced to ensure the UAVs' safety, but it will take longer for the UAV team to reach the desired formation. After the desired formation is achieved, the turning rate of the UAVs in the simulation is below 13.8 deg/s. The bank angle required to achieve this turning rate under the coordinated-turn assumption is around 10.3 degrees, which is reasonable for small fixed-wing UAVs.

The simulations also suggest that the required detection radius of the UAVs in cooperative track-

ing can be greatly reduced since the UAVs can get much closer to the GMT. In the single-UAV tracking scenario, the detection radius of the UAV needs to be greater than the loitering radius (200 m) if the UAV has to maintain continuous observation of the GMT. By contrast, the detection radius in cooperative tacking can be reduced to as low as 180.2 meters while still ensuring that the GMT is under the observation of at least one UAV at any time. If the detection radius is greater than 180.2 meters, more than one UAV would be observing the GMT concurrently sometimes, thus collecting more information of the GMT, which may lead to a better estimation of the GMT's states. This confirms the key benefits of the proposed cooperative tracking strategy: 1) enabling UAVs with a limited sensor coverage to perform persistent tracking through a formation, which may not be able to do so individually; 2) improving estimation performance through the cooperation of multiple sensors.

5.3 Comparative Study

As mentioned in preceding sections, the proposed loitering algorithm is capable of maintaining tracking of a GMT that is almost as fast as the UAV. In order to fully examine its superiority over existing loitering methods in this aspect, the proposed loitering algorithm is compared with a loitering algorithm that is based on the well-known LVF method. The LVF method was applied by several researchers in UAV-GMT tracking problems, and the one used in the comparative study is adopted from [3]. This approach constructs a vector field, which contains a limit circle centered at a target of interest and provides a desired velocity (e.g., heading and speed) for UAVs to converge to the limit circle from arbitrary initial positions. The velocity field essentially specifies the motion of the UAV with respect to the GMT. In fact, the relative speed between the UAV and the GMT at any point of the loitering circle is prescribed to be a constant. Figure 17 illustrates the two extreme cases of their relative motion, in which the two vehicles are moving in the same and opposite directions. The UAV's speed at these two locations, v_{a1} and v_{a2}, and the predefined relative speed, v_r, must satisfy $v_r = v_{a1} - v_t = v_{a2} + v_t$. Let $v_{a,min}$, and $v_{a,max}$ denote the UAV's minimum and maximum speeds, then the GMT's speed v_t must satisfy the following two constraints

$$v_t \leq v_{a,max} - v_r, \quad v_t \leq v_r - v_{a,min}$$

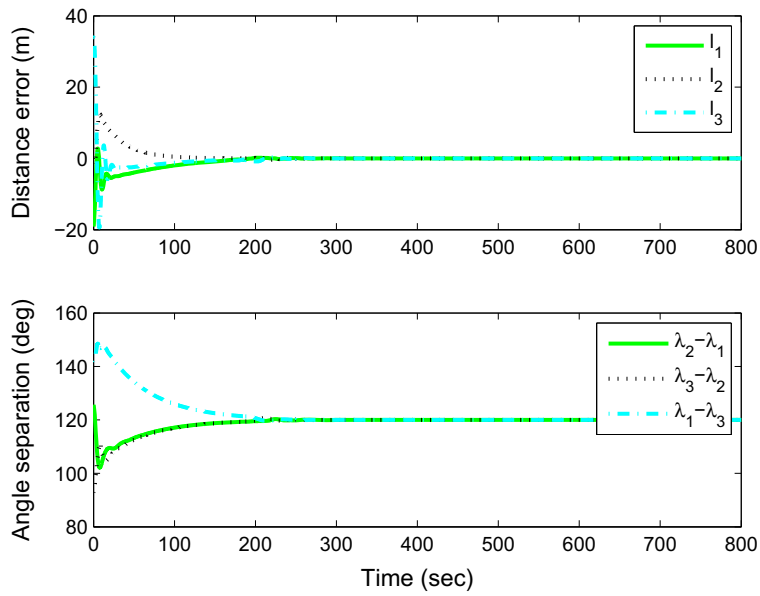

Fig. 14 Formation variables in tracking a GMT

Fig. 15 The relative distance between the GMT and UAVs

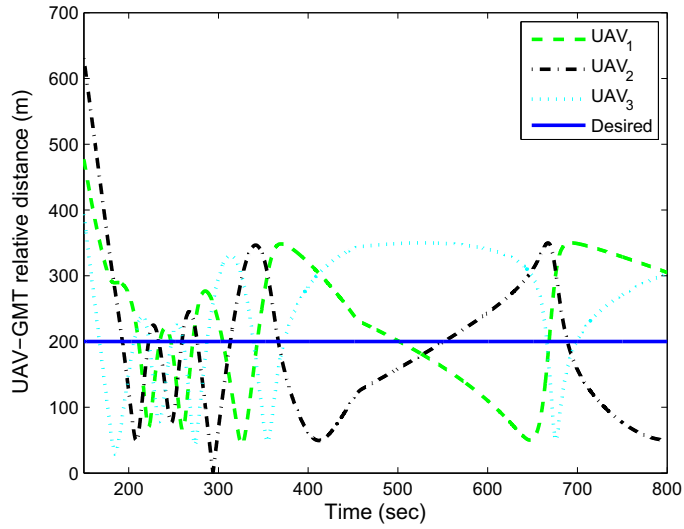

(a) Distance between the GMT and UAV individuals

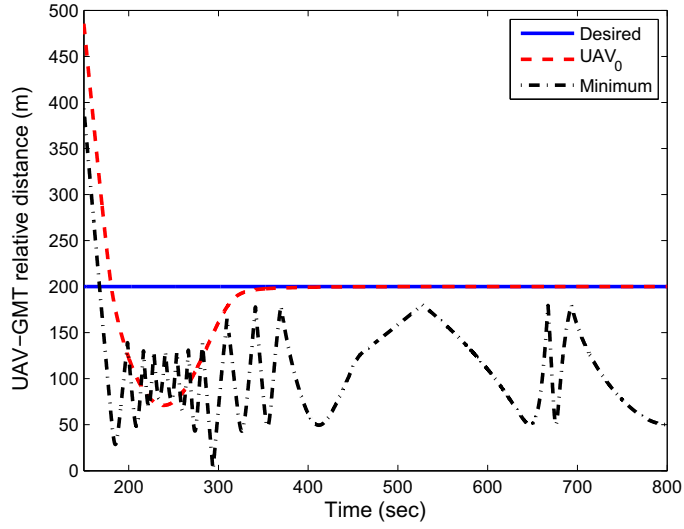

(b) Distance to the formation center and distance to the closest UAV

which indicate that the maximum speed of the GMT is $(v_{a,max} - v_{a,min})/2$, provided that the relative speed v_r is set to be $(v_{a,max} + v_{a,min})/2$.

The GMT's speed limit of the LVF method identified above is significantly smaller than the UAV's maximum speed; therefore, this method is only applicable to slow targets. This study will further compare these two algorithms by examining the UAV's motion when they are applied in a tracking task with a GMT varying its speed over a large range. The GMT motion profile shown in Fig. 4 is applied to the LVF method with the desired loitering radius set as 200 m. The relative speed in the LVF method is set as 13 m/s so that the UAV would fly at this speed in the case of a

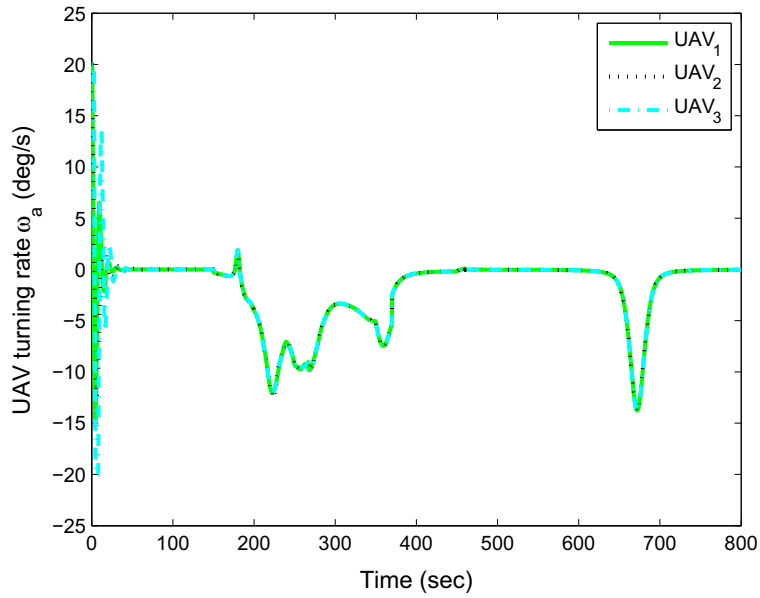

Fig. 16 UAV turning rates in tracking a GMT

stationary target. The UAV speeds resulting from the two algorithms are presented in Fig. 18. As shown, the UAV's speed of the LVF method is varying from 1 m/s to 25 m/s, conforming to what was found in the preceding paragraph. This wide speed range is very likely to violate the kinematic constrains of fixed-wing UAVs. The lower bound of the speed range is so small that it will cause a stall. In addition, the speed changes rather quickly in a large range, so it presents a formidable task for the UAV's flight controller to maintain such motion. The UAV's turning rates shown in Fig. 19 further shows that the LVF loitering algorithm is infeasible to be implemented on a real fixed-wing UAV under the current configuration. In order to reduce the magnitude of the UAV's turning rate, the loitering radius needs to be significantly increased. The relative distance shown in Fig. 20 demonstrates comparable performance of these two algorithms in converging to the loitering circle. As shown in these figures, the UAV's motion resulting from the LVF method is within reasonable range in the first 300 seconds when the GMT is moving at 2 m/s. As the GMT's speed increases, the UAV needs to take very aggressive maneuvers and to vary its speed quickly over a wide range in order to maintain loitering. These simulation results, along with the analytical result presented above, clearly confirm that the loitering algorithm based on the LVF method is only applicable to tracking tasks with slow targets.

The LVF-based loitering algorithm was extended in [5] to the multi-UAV cooperative tracking case. In this comparative study it is also compared with the proposed cooperative tracking algorithm in the same simulation configuration. The LVF-based

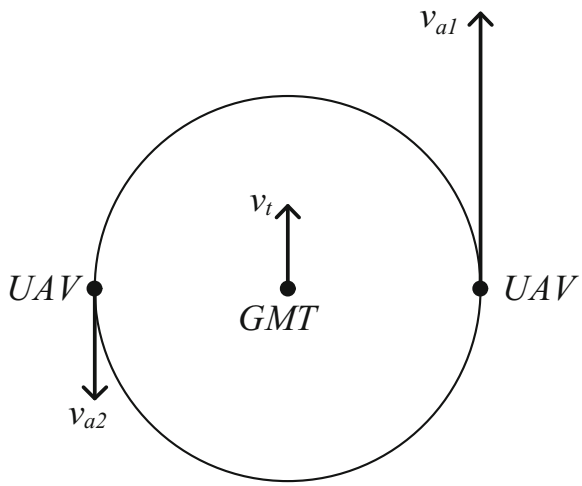

Fig. 17 UAV and GMT relative motion in two extreme cases of the LVF loitering ($v_{a,min} \leq v_{a1} \leq v_{a,max}$, $v_{a,min} \leq v_{a2} \leq v_{a,max}$)

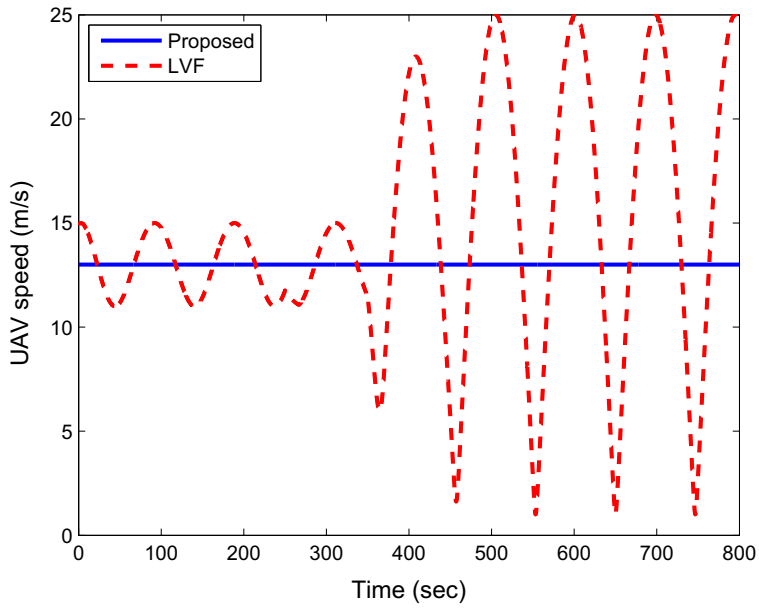

Fig. 18 UAV speed in the proposed and LVF tracking algorithms

loitering algorithm is augmented in [5] to include a motion coordination component that varies both the UAV speeds and turning rates in order to regulate the inter-vehicle angular separation. The simulation configuration described in the previous section is used for the LVF cooperative loitering algorithm, and the results are presented in Figs. 21, 22, 23 along with corresponding simulation results obtained by the proposed cooperative tracking algorithm. Because the behavior of all three UAVs in each algorithm is very similar to each other, these figures only compare the motion of the first UAV from each algorithm for the sake of brevity. As can be seen from the UAV's speeds in Fig. 21 and the turning rates in Fig. 22,

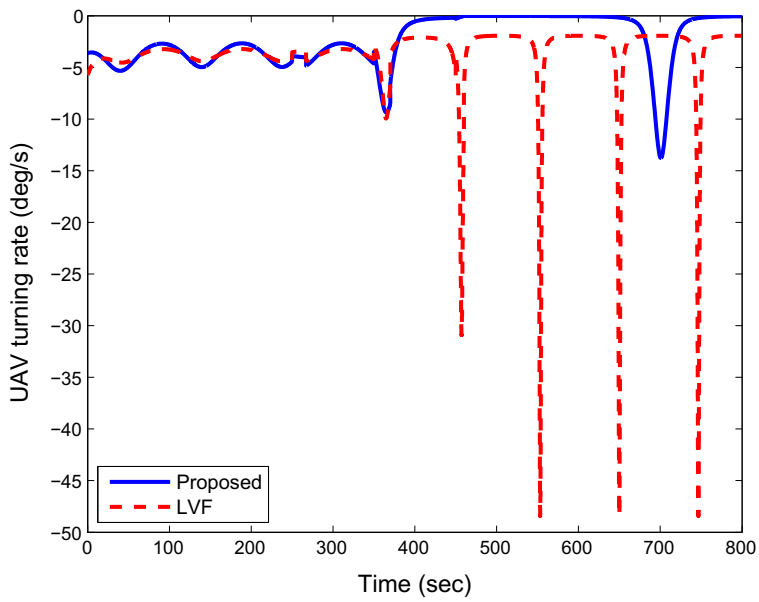

Fig. 19 UAV turning rate in the proposed and LVF tracking algorithms

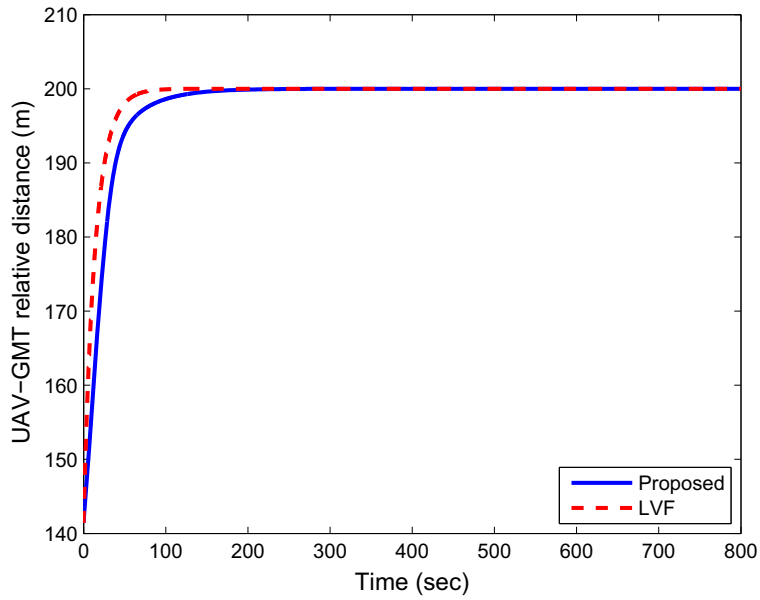

Fig. 20 UAV-GMT distance in the proposed and LVF tracking algorithms

the LVF cooperative loitering algorithm requires very aggressive motion of the UAVs in order to evenly distribute the UAVs on the loitering circle, while the proposed algorithm allows the UAVs to fly at a constant speed with moderate maneuvers. The relative distance between UAV_1 and the GMT in the LVF algorithm is compared with that in the proposed algorithm in Fig. 23, which also shows the minimum distance achieved by the proposed algorithm. As aforementioned, the relative distance resulting from the

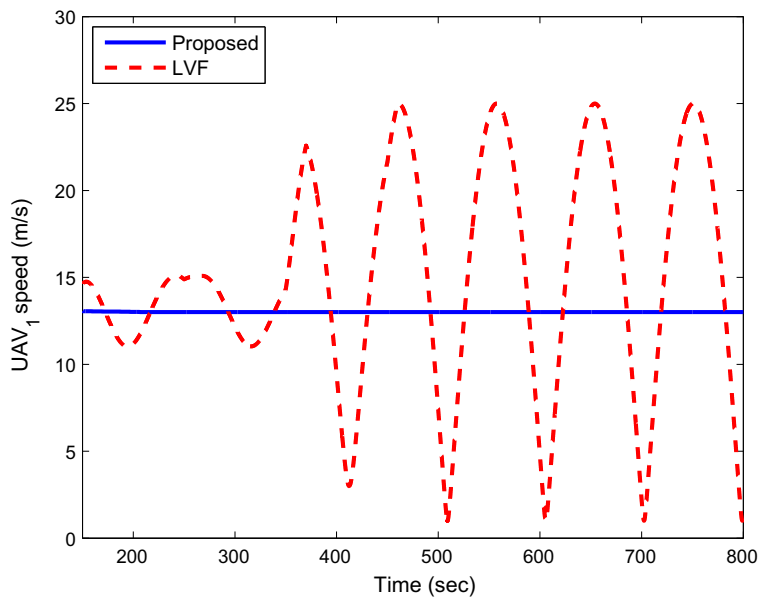

Fig. 21 Speed of UAV_1 in the proposed and LVF cooperative tracking algorithms

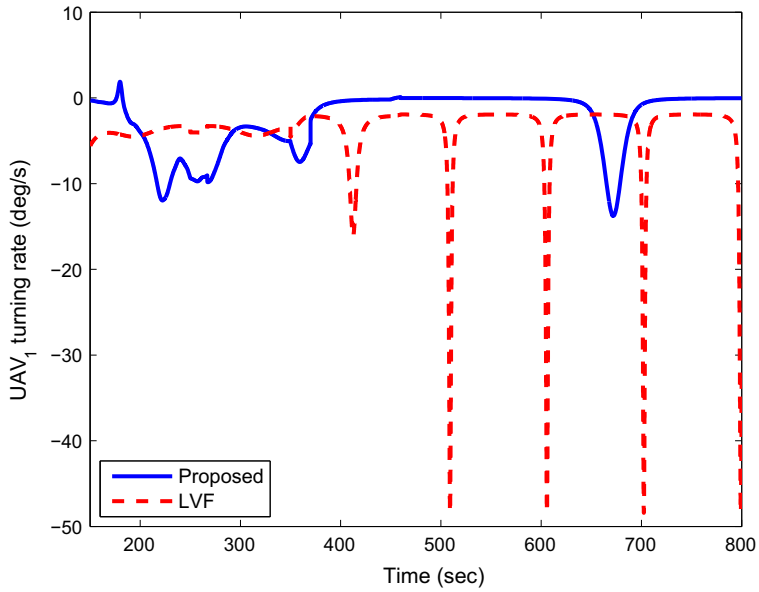

Fig. 22 Turning rate of UAV_1 in the proposed and LVF cooperative tracking algorithms

proposed algorithm is time-varying, but it is guaranteed that there is one or more UAVs within the desired loitering radius at any time instant. The LVF algorithm guides all UAVs to stay on the loitering circle, so the relative distance becomes constant in steady state. This configuration is highly advantageous for target observation, but it requires the UAVs to be very maneuverable and be able to vary their speeds over a large range.

The comparative study confirms that the proposed algorithms are superior to existing methods in tracking a fast target. Under the proposed algorithms, the GMT

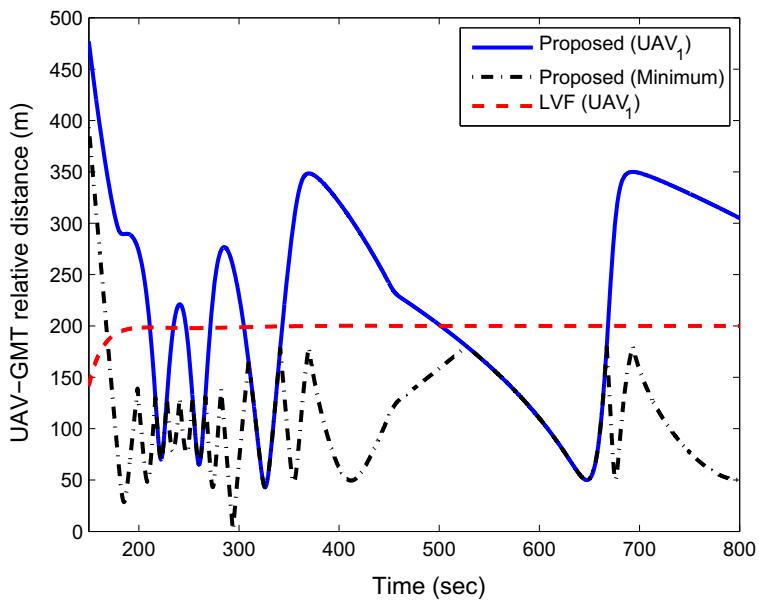

Fig. 23 UAV-GMT distance in the proposed and LVF cooperative tracking algorithms

is allowed to be almost as fast as the UAV, while the UAV can fly at a constant speed and its turning rate is moderate.

6 Conclusions

This paper developed a cooperative tracking scheme that allows multiple fixed-wing UAVs to track a GMT. It is built in a two-layer structure, containing a loitering algorithm and a formation algorithm. The former enables target tracking using a single UAV, while the latter enables multi-UAV cooperation in target tracking.

The proposed loitering algorithm is based on sliding mode control, and it significantly simplifies the control strategy by only regulating the distance between the UAV and the GMT and leaving the circling angular velocity as a free parameter. Under this strategy, a fixed-wing UAV can fly at a constant speed to maintain loitering by only manipulating its turning rate, while the GMT being tracked is allowed to vary its speed over a wide range and can be almost as fast as the UAV. The formation algorithm was developed to coordinate the motion of multiple fixed-wing UAVs to perform target tracking in a cooperative manner. Based on virtual structure, it guides multiple UAVs to fly in a circular formation with equal inter-vehicle angular separation and keeps the UAV team behaving as a single, virtual UAV. The loitering algorithm was applied to a multi-UAV team through implementing it on this virtual UAV, and the admissible range of the GMT's speed was not affected. This formation strategy was designed in a special way such that it does not cause additional requirements on the motion capability of the UAVs, regardless of the task assigned to the UAV team. In other words, the formation strategy and the task assigned to the team are independent of each other, and they can be designed separately. An integration of these two components would not affect each other's individual function. As a result, this strategy is not limited to the target tracking task studied in this paper; it can be applied to other UAV missions as well. In fact, existing UAV control techniques involving a single UAV can be directly applied to a multi-UAV team under this formation strategy by implementing them on the virtual UAV.

In the proposed formation algorithm, the information of inter-vehicle separation angles can be exchanged among the UAV network locally, but all the rest information needs to be shared globally. This algorithm is therefore only partially distributed. A fully distributed implementation of this algorithm can reduce the amount of information communicated within the UAV network and increase its scalability, which is worth further investigation in the future development of this work. Another problem that should be considered in the future is related to the target states. In the proposed cooperative tracking system, UAVs need to know the GMT's states, including its position, velocity, and acceleration. Therefore, the next endeavor of this work should explore the possibility of using an onboard observation sensor such as a camera to facilitate tracking.

Acknowledgements This work was supported by the Natural Sciences and Engineering Research Council (NSERC) of Canada under Strategic Project Grant 350978.

References

1. Sarris, Z.: Survey of UAV applications in civil markets (2001). In: The 9th IEEE Mediterranean Conference on Control and Automation (MED '01), Croatia (2001)
2. Elston, J., Frew, E.W.: Hierarchical distributed control for search and tracking by heterogeneous aerial robot networks. In: 2008 IEEE Internation Conference on Robotics and Automation, pp. 19–23, CA, USA (2008)
3. Frew, E.W., Lawrence, D.A., Morris, S.: Coordinated standoff tracking of moving targets using Lyapunov guidance vector fields. J. Guid., Control Dyn. **31**(2), 290–306 (2008)
4. Summers, T.H., Akella, M.R., Mears, M.J.: Coordinated standoff tracking of moving target: Control laws and information architectures. J. Guid., Control Dyn. **32**(1), 56–69 (2009)
5. Lim, S., Kim, Y., Lee, D., Bang, H.: Standoff target tracking using a vector field for multiple unmanned aircrafts. J. Intell. Robot. Syst. **69**(1-4), 347–360 (2012)
6. Lee, J., Huang, R., Vaughn, A., Xiao, X., Karl Hedrick, J., Zennaro, M., Sengupta, R.: Strategies of path-planning for a UAV to track a ground vehicle. In: The Second Annual Symposium on Autonomous Intelligent Networks and Systems, CA, USA (2003)
7. Dobrokhodov, V.N., Kaminer, I.I., Jones, K.D.: Vision-based tracking and motion estimation for moving targets using unmanned air vehicles, vol. 31, pp. 907–917 (2008)
8. Ponda, S., Kolacinski, R., Frazzoli, E.: Trajectory optimization for target localization using small unmanned aerial vehicles. In: AIAA Guidance, Navigation, and Control Conference, Chicago, Illinois (2009)
9. Spry, S.C., Giard, A.R., vehicles, J., Hedrick, K.: Convoy protection using multiple unmanned aerial vehicles:

Organization and coordination. In: 2005 American Control Conference, pp. 3524–3529, OR, USA (2005)
10. Zhang, M., Liu, H.H.T.: Vision-based tracking and estimation of ground moving target using unmanned aerial vehicle. In: 2010 American Control Conference, MD, USA (2010)
11. Oliveira, T., Encarnação, P.: Ground target tracking for unmanned aerial vehicles. In: AIAA Guidance, Navigation, and Control Conference, Toronto, Ontario, Canada (2010)
12. Xiaowei, F., Feng, H., Gao, X.: UAV mobile ground target pursuit algorithm. J. Intell. Robot. Syst. **68**, 359–371 (2012)
13. Zhang, M., Liu, H.H.T.: Persistent tracking using unmanned aerial vehicle: A game theory method. In: AIAA Guidance, Navigation, and Control Conference, Portland, Oregon (2011)
14. Zhang, M., Liu, H.H.T.: Game-theoretical persistent tracking of a moving target using a unicycle-type mobile vehicle. IEEE Trans. Industrial Electronics **61**(11), 6222–6233 (2014)
15. Kim, S., Ohy, H., Tsourdos, A.: Nonlinear model predictive coordinated standoff tracking of moving ground vehicle. In: AIAA Guidance, Navigation, and Control Conference, Portland, Oregon, August 8–11 2011. AIAA 2011–6312
16. Zhang, M., Liu, H.H.T.: Moving target tracking by unmanned aerial vehicle: A model predictive control method. In: Canadian Aeronautics and Space Institute AERO'11 Conference, pp. 26–28, Quebec, Canada (2011)
17. Martínez, S., Bullo, F.: Optimal sensor placement and motion coordination for target tracking. Automatica **42**(4), 661–668 (2006)
18. Zhang, M., Liu, H.H.T.: Vision-based estimation of ground moving target by multiple unmanned aerial vehicles. In: 2012 American Control Conference, pp. 27–29, Quebec, Canada (2012)
19. Hyondong, O., Kim, S., Tsourdos, A., White, B.A.: Decentralised standoff tracking of moving targets using adaptive sliding mode control for UAVs. J. Intell. Robot. Syst. **76**, 169–183 (2014)
20. Kingston, D., Beard, R.: UAV splay state configuration for moving targets in wind. In: Advances in Cooperative Control and Optimization, pp. 109–128. Springer (2007)
21. Zhang, M., Liu, H.H.T.: Aerodynamics and flight control of flying-wing unmanned aerial vehicles. In: Canadian Aeronautics and Space Institute Aero'13 Conference, Ontario Canada (2013)
22. Ren, W., Beard, R.W.: Trajectory tracking for unmanned air vehicles with velocity and heading rate constraints. IEEE Trans. Control Syst. Technol. **12**(5), 706–716 (2004)
23. Khalil, H.K. Nonlinear systems, 3rd. Prentice Hall, Upper Saddle River, NJ (2002)
24. Bethke, B., Valenti, M., How, J.: Cooperative vision based estimation and tracking using multiple UAVs. In: Proceedings of the Conference on Coopetative Control and Optimization, Gainesville, FL (2007)
25. Campbell, M.E., Whitacre, W.W.: Cooperative tracking using vision measurements on SeaScan UAVs. IEEE Trans. Control Syst. Technol. **15**(4), 613–626 (2007)
26. Ridley, M., Nettleton, E., Göktogan, A., Brooker, G., Sukkarieh, S., Durrant-Whyte, H.F.: Decentralised ground target tracking with heterogeneous sensing nodes on multiple UAVs. In: Information processing in sensor networks, pp. 545–565. Springer (2003)
27. Olfati-Saber, R., Alex Fax, J., Murray, R.M.: Consensus and cooperation in networked multi-agent systems. IEEE Proc. **95**(1), 215–233 (2007)

Mingfeng Zhang received the B.E. and M.E. degrees from Beihang University (formerly Beijing University of Aeronautics and Astronautics), Beijing, China, in 2005 and 2008, respectively, and the Ph.D. degree in aerospace science and engineering from the University of Toronto, Toronto, ON, Canada, in 2013.

He is currently a Postdoctoral Fellow with the Department of Mechanical Engineering, McGill University, Montreal, QC, Canada. His research interests include autonomous navigation and flight of unmanned aerial vehicles, and vision-based control and estimation.

Hugh H. T. Liu received the Ph.D. degree in mechanical engineering from the University of Toronto, Toronto, ON, Canada, in 1998. He is currently a Professor with the University of Toronto Institute for Aerospace Studies, Toronto. His research interests include aircraft systems and control related areas.

Dr. Liu is a Fellow of the Canadian Society for Mechanical Engineering, an Associate Fellow of the American Institute of Aeronautics and Astronautics, and an Active Member of the Canadian Aeronautics and Space Institute. Dr. Liu is also a registered Professional Engineer in Ontario. He also serves on editorial and technical committees of international professional societies.